HHS Public Access

Author manuscript

Int J Hyperthermia. Author manuscript; available in PMC 2017 November 01.

Published in final edited form as:

Int J Hyperthermia. 2016 November ; 32(7): 786–794. doi:10.1080/02656736.2016.1197972.

MRI-guided Focused Ultrasound Ablation of Lumbar Medial Branch Nerve: Feasibility and Safety Study in a Swine Model

Elena A Kaye[1], **Sebastien Monette**[2], **Govindarajan Srimathveeravalli**[3], **Majid Maybody**[3], **Stephen B Solomon**[3], and **Amitabh Gulati**[4]

[1]Department of Medical Physics, Memorial Sloan Kettering Cancer Center, New York, USA

[2]Tri-Institutional Laboratory of Comparative Pathology, Memorial Sloan Kettering Cancer Center, The Rockefeller University, Weill Cornell Medical College, New York, USA

[3]Department of Radiology, Memorial Sloan Kettering Cancer Center, New York, USA

[4]Department of Anesthesiology, Memorial Sloan Kettering Cancer Center, New York, USA

Abstract

Purpose—About 10–40% of chronic low back pain cases involve facet joints, which are commonly treated with lumbar medial branch (MB) radiofrequency neurotomy. Magnetic Resonance Imaging-guided Focused Ultrasound (MRgFUS), a non-invasive, non-ionizing ablation modality used to treat tumors, neuropathic pain and painful bone metastasis, can also be used to disrupt nerve conduction. This work's purpose was to study the feasibility and safety of direct MRgFUS ablation of the lumbar MB nerve in acute and subacute swine models.

Materials and Methods—In vivo MRgFUS ablation was performed in six swine (3 acute and 3 subacute) using a clinical MRgFUS system (ExAblate 2000®; InSightec Ltd., Haifa, Israel) and 3 T MRI scanner (SIGNA; GE Healthcare, Waukesha, WI, USA) combination. Behavioral assessment was performed, and imaging and histology were used to assess the treatment.

Results and Conclusions—Histological analysis of the in vivo studies confirmed thermal necrosis of the MB nerve could be achieved without damaging the spinal cord or adjacent nerve roots. MRgFUS did not cause changes in the animals' behavior and ambulation.

Keywords

HIFU; FUS; MRI-guided; nerve ablation; swine model; facet joint

Introduction

Chronic Low Back Pain (CLBP) is one of the most common causes of disability in U.S. adults. Between 10 and 40% of CLBP cases involve zygapophyseal, i.e., facet joints [1, 2] and are commonly treated with percutaneous lumbar medial branch (MB) radiofrequency neurotomy (RFN). While RFN is the most common method of MB neurolysis, it frequently

Correspondence to: Amitabh Gulati, gulatia@mskcc.org. 1275 York Ave, New York, NY 10065. 212-639-6851.

Declaration of interest statement

The rest of the authors report no declarations of interest.

relies on fluoroscopic image guidance and requires percutaneous needle placement at the desired location.

Magnetic Resonance Imaging (MRI)-guided Focused Ultrasound (MRgFUS) is a non-invasive, non-ionizing ablation modality, which is used to treat various tumors [3–5], neuropathic pain [6] and painful bone metastasis [7]. Additionally, multiple research studies have focused on the ability of FUS to disrupt nerve conduction and cause necrosis of nerves [8, 9], including MRgFUS renal sympathetic denervation [10], abltation of sciatic [11, 12] and intercostal [13] nerves.

To develop an MRgFUS application for facet joint pain treatment, two recent studies demonstrated safety and feasibility of MRgFUS ablation in preclinical [14] and clinical [15] settings. In an 18-patient group treated with MRgFUS, 60.2 % and 51.2 % of patients reported a reduction of average and worst pain, respectively[15]. The lack of pain score improvement in the remaining patients may be explained by the selected targeting strategy. In these studies, rather than directing the FUS beam at the MB nerve (as is commonly done during RFN), to avoid interaction of the FUS beam with critical structures, such as the spinal cord and the nerve root, the FUS beam targeted the facet joint itself, and aimed to achieve denervation by ablating the peri-articular tissue and the nerves inside it (Fig 1A). Success of such a strategy relies on ablation of all small nerves innervating the joint (essentially the entire joint capsule), and may be compromised by the inability to visualize each nerve and thus verify its destruction.

An alternative targeting strategy is to adopt the approach used in RFN and aim the FUS beam directly at the MB nerve (Fig 1B). Feasibility of such an approach can be hypothesized based on the acoustic properties of bone and clinical experience with RF ablation in the spine. Due to its high density and heterogeneous composition, bone tissue reflects and attenuates ultrasound [16, 17] at a much greater rate than muscle. This enables the spine bone to minimize the intensity of the ultrasound beam, especially the far-field, which may reach the spinal canal. The protective role of spinal fluid and the venous plexus, reported in spine RF ablation studies [18–20], further decreases the risk of thermal damage occurring in the spinal cord or adjacent nerve roots. These properties, combined with the diminished heat transmission of cortical and cancellous bone [18], provide a theoretical foundation for the feasibility of direct targeting the MB nerve with focused ultrasound.

Hence, we hypothesize that direct MRgFUS ablation can be used safely and effectively on the lumbar MB nerve, and our study's purpose was to test this hypothesis using a clinical MRgFUS system and a swine animal model.

Materials and Methods

Acute (animals were euthanized immediately following the procedure) and subacute (euthanized 48 hours following the procedure) in vivo studies were conducted to evaluate the feasibility and safety of MRgFUS ablation of the MB nerve. As topography of medial branch nerve in swine was not previously reported, first, a preliminary ex vivo investigation was performed to study the location and the size of the nerve using histology and MRI. All

animal procedures received approval from the Institutional Animal Care and Use Committee. Appropriate handling and care was provided by trained staff in accordance with the principles of laboratory animal care and guidelines from the United States Department of Agriculture. Descriptive statistics were employed to summarize the results.

Ex Vivo Study of Lumbar Medial Branch Nerve Topography

To investigate the topography of the MB nerve in Yorkshire swine, a freshly harvested porcine lumbar spine was used. First, the nerve was studied using histological analysis, and then nerve position was imaged using MRI. For histological assessment, the tissue was prepared and processed as described in the Histology section. Serial sectioning of the tissue was performed, to sample the anatomy every 100 μm. A separate sample of freshly excised section of porcine spine was imaged on a 3 Tesla MRI scanner (Discovery MR750, GE Healthcare, Milwaukee, WI, USA) using a spine RF coil. The short tau inversion recovery (STIR) sequence, common in neurography [21], was used. Slice thickness was 2 mm and in-plane resolution was 0.5 mm by 0.7 mm (field of view was 18 cm and matrix size was 384 by 256). Echo time was 43.3 ms, inversion time was 225 ms, repetition time was 5300 ms, number of averages was 2 and the total scan time for 54 slices was 14.5 minutes.

MRgFUS System

A clinical FUS system (ExAblate 2000®; InSightec, Ltd., Haifa, Israel) installed in a 3 Tesla MRI scanner (SIGNA; GE Healthcare, Waukesha, WI, USA) was used. A polyacrylamide gel pad was used for acoustic coupling between the tissue and FUS transducer bath (Fig 2A). Imaging was performed using a body transmit/receive radiofrequency (RF) coil. The central frequency of focused ultrasound was increased to 1.35 MHz to minimize ultrasound penetration into bone tissue, as previously proposed by Harnof, et al. [14], and the focal spot type was set to short. The default values of sonication duration, 20 s, and cooling time were automatically calculated by the treatment planning software and was 90 s or longer. The treatment was monitored in near real-time using rapid acquisition of MR images, from which temperature maps were calculated by the planning software (InSightec, Ltd.) based on proton resonance frequency shift (PRFS) baseline subtraction approach [22] (Fig 2B). As the current method for MR thermometry is not sensitive to the MRI signal coming from cortical bone, the temperature was monitored in muscle adjacent to bone.

Acute and Subacute Study of Medial Branch Nerve MRgFUS Ablation

Animal Protocol—Six female Yorkshire swine (30–37 kg) underwent MRgFUS ablation of MB nerves. In each animal, skin hair was removed from the lumbar region using a razor and hair removal cream (Nair™; Church & Dwight Co., NJ, USA). As per protocol, each animal was sedated with telazol (4.4 mg/kg) and glycopyrrolate (0.007 mg/kg), and was anesthetized by subcutaneous injection of carprofen and intravenous injection of buprenorphine. The animals were intubated and a surgical plane of anesthesia was maintained using Isoflurane 2–3% with 100% oxygen on a Penlon Nuffield MRI-compatible ventilator (Penlon, Inc., Minnetonka, MN, USA). Heart rate and pulse oximetry were continuously monitored. All animals were euthanized with an overdose via intravenous injection of Euthasol while under anesthesia. Three animals were euthanized immediately

following the procedure (acute study) and three animals were euthanized 48 hours after (subacute study). In the subacute study, the animals were maintained on preventative medications for potential pain following the treatment: meloxicam (0.4 mg/kg) was given every 24 hours and buprenorphine (0.01 mg/kg) was administered twice a day. Both pain and behavioral assessments, including evaluating ambulation and gait, were performed twice daily by the veterinary staff, who were blinded to treatment location side to minimize observer bias.

MRgFUS Treatment—The animals were placed on the MRgFUS table in a tilted, supine, feet-first position as shown in Fig 2A. Planning MR images of the lumbar spine were acquired using a T2-weighted sequence and loaded into a treatment planning workstation (InSightec Ltd.). An experienced, board-certified pain medicine anesthesiologist prescribed the treatment regions on images of the vertebral levels L2 through L6 (Fig 2B–C). For the acute study, a region of treatment was drawn manually and the MRgFUS treatment software automatically calculated the number and the locations of sonications necessary to ablate the defined region (Fig 2B). For the subacute study, individual sonications were prescribed in the space between the articular and transverse processes in up to three image slices (3 mm slice) (Fig 2B–C). The targeted vertebral levels (referred to as target), the number of sonications applied to each target, and the average acoustic energy per target are listed in Table 1. Multiple sonications were used to ensure that ablated region enclosed the nerve. However, due to time constraints, in the acute experiment 3, in one out of three targeted levels single sonication was applied. The acoustic energy of that sonication was increased to 1246 J. The focal distance ranged from 120 mm to 145 mm, depending on the weight of the animal and the position of the target. The length of the focal spot was between 11 mm and 12 mm for all animals except acute experiment 3, where overall higher energy was used and the focal spot length ranged from 14 mm to 19 mm. In the acute study, a total of fifteen nerve locations were targeted, and a total of nine were treated in the subacute study. Unilateral treatment was performed in five out of six animals so that the contralateral side could be used as internal control. In one acute case, the contralateral side was also treated due to the technical issues that compromised ablation targeting on one side (details are discussed in the Results section).

Treatment Assessment—The effects of MRgFUS treatment were evaluated using contrast-enhanced MR and Computerized Tomography (CT) imaging, pain and behavioral assessments and histopathology.

Contrast-enhanced MRI (CE-MRI) was performed immediately following the procedure, using intravenous gadopentetate dimeglumine MRI contrast agent (Magnevist®; Bayer HealthCare, Bayer AG, Leverkusen, Germany), 0.2 ml/kg (0.1 mmol/kg) and T1-weighted fast spoiled gradient-recalled echo imaging. In the subacute study, the animals were imaged on a CT scanner (Innova; GE Healthcare, Milwaukee, WI, USA) using iohexol contrast medium (Omnipaque 300; GE Healthcare, Milwaukee, WI, USA) 48 hours after treatment. Thermal necrosis was inferred from loss of tissue perfusion, as indicated by the lack of contrast uptake, in both MRI and CT imaging. Using axial CE-MRI or CE-CT images, the size of the lesions was measured along the hypotenuse between the transverse and articular

processes. CT images were used to measure the thickness of pedicle bone between the spinal canal and the junction of the transverse and the articular processes in three subacute cases and compared to the measurements carried out in the lumbar spine of two human adults.

In the subacute study, twice a day the veterinary staff observed the animals for any signs of pain, altered gait, abnormal posture, changes and asymmetry in movement. The veterinary staff was blinded to whether the treatment was performed on the left or right side of the animal. Pain assessment was performed via observation and palpation, both superficial and deep [23]. The skin was visually inspected for any potential burns.

To study the ablative effects on a cellular level, gross and histological analysis were performed. Tissue was processed as described in the Histology section. The slices containing the lesions were identified through gross visual inspection. For each lesion, 1 to 3 rectangular samples and the sections containing the nerve roots above and below the ablation site were analyzed (Fig 6). Histological analysis of the untreated side, control, was done to establish the normal appearance of all tissue types.

Histology

Tissue samples were processed according to the following steps. First, a section of lumbar spine, comprised of 4 or 5 vertebra levels and minimal muscle attached to the bone, was fixed by immersion in 10% neutral buffered formalin for approximately two to four weeks until complete fixation was achieved. Second, the specimen was placed into decalcifying solution Surgipath Decalcifier I (Leica Biosystems, Richmond, IL, USA) for four to five weeks. Upon complete decalcification, the sample was sectioned transversely into 5 mm thick slices and the nerves of interest were excised en bloc with adjacent muscle, bone and the spinal cord. These samples were processed routinely in alcohol and xylene, embedded in paraffin, sectioned at 5-micron thickness, and stained with hematoxylin and eosin.

Results

Ex Vivo Study of Lumbar Medial Branch Nerve Topography

The analysis of the histology sections showed that the MB nerve arises from the dorsal ramus and runs caudally and dorsally adjacent to the bone at the junction of the superior articular and transverse processes (Fig 3A). The transverse dimensions of the nerve were approximately 400–650 μm by 200–300 μm and it was positioned approximately 100–200 μm away from the bone surrounded by an approximate 200 μm layer of adipose tissue. The high resolution MR image did not clearly resolve the nerve, however, the region where nerve and the “pocket” of adipose tissue surrounding it were located could be readily identified in the images (Fig 3B). These findings informed targeting of the MB nerves in the subsequent in vivo experiments.

Acute and Subacute Study of Medial Branch Nerve Ablation

Unilaterally, four to five lumbar vertebrae levels could be accessed by the FUS transducer without the need to reposition the animal. The peak temperatures per sonication achieved in

each target during treatment are summarized in Table 1. On average, the peak temperatures of 55 C and higher were achieved in each target.

Follow-Up Imaging

The results of the study showed that thermal lesions in muscle were well-delineated on contrast-enhanced imaging using both MRI and CT. Changes in contrast uptake in adjacent bone was faintly discernible on CE-MRI (Fig 5B), but not distinguishable on CE-CT images. Nineteen out of 24 treatments resulted in thermal lesions positioned between the transverse and articular processes, as prescribed (Fig 4). When the focal region of a sonication was not precisely between the articular and transverse processes, heating of the processes occurred and resulted in a reduction of contrast uptake in and around the bone (Fig 5A–C). The change in position of the animal that occurred during acute experiment 3 was not accounted for intra-procedurally, and resulted in the lateral shift of five ablations approximately 10 mm away from their target position (Fig 5D). These five cases were excluded from further analysis. The extent of the muscle lesions ranged from 0.6 cm to 2.6 cm in the acute study, and from 0.9 cm to 1.4 cm in the subacute study. As the length of the FUS focus increases with increasing acoustic energy, the largest lesions were created while using acoustic energy greater than 900 J. The thickness of the pedicle bone, measured as a distance between the spinal canal and the junction of the transverse and articular processes, ranged from 8.5 mm to 12 mm, increasing between L1 and L6. For comparison, lumbar pedicle bone thickness was 13–16 mm in a 70-kg female and 17–21 mm in a 102-kg male.

Gross Pathology and Histology

On gross pathology (Fig 6), in the acute cases, the targeted region appeared pale and was difficult to differentiate from the normal tissue, whereas in the subacute cases, thermal damage was more readily observed with hemorrhage presenting as a brown rim surrounding the pale ablation region in muscle tissue and penetrating several millimeters into the bone. The gross appearance of nerve root slices was normal in both acute and subacute studies. In all six animals, no skin burns were found. The extent of changes in bone ranged from 2.6 mm to 4.3 mm in subacute animal 1, in animal 2 – from 2.6 mm to 2.8 mm, and in animal 3 - from 3 mm to 3.6 mm.

Histological analysis showed that, on low magnification, the rim of hemorrhage and macrophages presence formed around the ablation made the thermal lesion more discernible (Fig 7). Changes in bone tissue, also clearly distinguishable on gross pathology (Fig 6C, 7), did not extend deep towards the spinal cord, leaving 5 to 7 mm of intact bone between the ablation and the spinal canal. All treatments resulted in thermal necrosis of the muscle tissue. Compared to untreated tissue, ablation presented as swelling of skeletal muscle fibres, sarcoplasmic hypereosinophilia and fragmentation, and nuclear shrinkage, with additional accumulation of macrophages at the lesion periphery and necrosis of the small vessels found in the subacute study only (Fig 8A–C). In acute and subacute studies, the ablated nerve exhibited at least one, and often a combination, of the following changes: hyalinization of epineurial collagen, hyperemia of endoneurial vessels, nuclear pyknosis of Schwann cells, and loss of axons associated with dilation of the myelin sheath (Fig 8D–F). Compared to the control side, bone and bone marrow adjacent to the nerve exhibited cellular

shrinkage, cytoplasmic hypereosinophilia and nuclear pyknosis of periosteal osteoblasts and hematopoietic cells, necrotic vessels and hemorrhage consistent with coagulative necrosis (Fig 9). The spinal cord and nerve roots appeared normal in all specimens.

Behavioral Assessment

During the post-procedural 48-hour period, neither changes in animal behavior nor function were observed, and no signs of superficial or deep pain were detected. In addition, there was no difference in the animals' ambulation, gait, or pain between the treated and untreated sides.

Discussion

This work evaluated the feasibility and safety of direct MRgFUS ablation of the lumbar MB nerve. The results demonstrate that MRgFUS can create thermal necrosis of the MB nerve, including the lowest lumbar vertebral level (L6), with minimal thermal damage to the adjacent muscle tissue and bone, without changes in the nerve root or the spinal cord, and without behavioral changes. This direct targeting of the MB nerve, currently used in RF neurotomy, as opposed to the targeting of the nerve endings on the facet joint surface [14, 15], can help ensure that innervation of the joint is disrupted and reduce the likelihood of incomplete treatment.

Analysis of histological sections and MR images of the ex vivo porcine lumbar spine demonstrated that the topography of the MB nerve was similar to that reported in humans [24], confirming the appropriateness of this animal model for a pre-clinical MB nerve ablation study. The lumbar vertebral body shape and size in the swine model are comparable to the lumbar spine of two examined human adults. Based on the similarity of the anatomical lumbar spine structures of the swine and human, it appears that direct MRgFUS targeting of the MB nerve and the acoustic parameters explored here could be clinically adapted.

Prior studies demonstrated that thermal ablation of the spine using RF devices did not harm the spinal cord in ex vivo and clinical studies [18, 20]. Additionally, a parametric patient-specific modeling of interstitial FUS ablation of vertebral tumors using a percutaneous 7 MHz ultrasound device [25] showed that tumors positioned at least 5 mm from the sensitive neural elements could be safely treated. When targeting the MB nerve using an extracorporeal FUS system, the cortical bone of the vertebral body and the transverse and superior articular processes are likely to serve as natural absorbers of ultrasound energy, preventing a significant portion of the far-field ultrasound beam from reaching the critical neural structures. Nonetheless, when using the clinical FUS system, which operates at a lower frequency of 1.35 MHz, an obvious concern is inadvertent damage of the spinal cord or exiting nerve root structures, which typically precludes the clinical application of MRgFUS in patients with spinal tumors [26]. In this work, the in vivo acute study demonstrated that the selected acoustic parameters and the targeting strategy did not damage the spinal cord and the lumbar nerve roots. These findings enabled progression of the study into a subacute animal model, in which assessment of any potential behavioral changes could be performed in addition to follow-up imaging and histology. No changes observed in animal function, ambulation, gate, or behavior, were consistent with lack of cellular change

in the spinal cord and the nerve roots. This lack of functional impact provides convincing initial evidence of the safety of direct MRgFUS ablation of the MB nerve.

Histology showed thermal damage of the targeted nerve in both the acute and subacute settings. The MB nerve exhibited nuclear pyknosis of Schwann cells and dilated myelin sheaths, which is consistent with prior studies of FUS ablation of the sciatic nerve in acute rabbit and swine models [8, 11]. Forty-eight-hour survival post-treatment provided time for macrophages and hemorrhage changes to evolve at the boundary of the lesion, which helped clearly delineate the extent of FUS penetration into the spine. The lack of cellular changes in the nerve roots, above and below the ablation region, demonstrate that it is feasible to deliver focused ultrasound to the lumbar MB nerve in a controlled manner, making this ablation modality very attractive for noninvasive treatment of low back pain.

In a typical MRgFUS treatment, a physician contours the region of treatment using MR images, and then, the planning software automatically determines the sonications necessary to deliver lethal thermal dose to the treatment region. In the case of the sub-millimeter MB nerve, the concept of region of treatment contour is less relevant, and it may simplify the workflow if sonications are prescribed individually. To avoid unwanted heating of the transverse and articular processes the roll and the pitch of the transducer can be adjusted. In this study, the undesired thermal necrosis of the adjacent bone was minimal, and is likely to resolve over time due to bone remodelling that occurs following FUS ablation [7, 27]. When selecting the optimal position of the focal point, it is important to consider the proximity to the nerve roots. In this study, to minimize the extent of ablation towards the nerve roots, the focus was placed at the interface between bone and muscle. This is in contrast to placing the focus behind the bone-muscle interface as is done during MRgFUS treatment of painful bone metastasis. In future studies, it would be valuable to explore the near-field targeting, as to determine the optimal position of the focal spot that achieves desired ablation coverage without affecting the nerve roots.

In the preliminary ex vivo investigation, this study demonstrated that high-resolution MRI can be used to visualize the MB nerve, normally not visible on X-ray fluoroscopy or ultrasound. Unfortunately, the current setup of the clinical MRgFUS system is not compatible with the spine RF coil and relies on the body RF coil for imaging. Due to the limited sensitivity of the body coil, visualization of the MB nerve was not feasible during the in vivo experiments. Developing FUS-compatible RF coils and increasing the sensitivity of MR neurography techniques [12, 28, 29] is essential to leveraging the superior imaging capabilities of MRI for this application. MR thermometry was valuable in this application as it depicted temperature changes in muscle adjacent to the bone. To enable MR thermometry in bone, recent studies explored the relationship between several MRI parameters and temperature of both bone, and bone marrow. Incorporation of MR thermometry techniques sensitive to temperature changes in bone may further improve precision of this treatment.

Translating of FUS-based neurolysis into the field of pain medicine, will require optimizing the treatment parameters and improving the procedure workflow. This study demonstrated that thermal damage of MB nerve could be achieved with minimal damage to adjacent bone and muscle using ultrasound frequency of 1.35 MHz, multiple sonications and an acoustic

energy of 600–700 J. To further minimize ablation of bone and muscle, it would be valuable to evaluate and optimize the treatment parameters such as ultrasound frequency, acoustic energy, focal spot type and the number of sonications. Additionally, reliable patient positioning is needed to prevent bulk movement of the patient. An optimized anesthesia protocol is essential to ensure patient comfort during the FUS procedure while still allowing sensory and motor testing. Finally, new devices that enable FUS neurolysis under less costly imaging guidance (compared to MRI), e.g., fluoroscopic or ultrasound imaging, will help to increase the utilization of this otherwise promising pain management modality.

The porcine anatomy, specifically the exaggerated curvature of the spine as compared to that of a human, and its quadruped stance, makes supine and tilted-supine positioning and immobilization of the limbs within the MRI scanner bore more technically challenging than would be expected for a human patient. Without secure immobilization, the animal can easily tilt from supine into a lateral position. The occurrence of such tilt in a position of one animal was unaccounted for and led to the lateral shift of the lesions. While positioning of the human subject would not face similar challenges, for further clinical utilization of MRgFUS in humans, intra-procedural movement will need to be minimized by reliable immobilization of the patient and careful monitoring of MR images for any changes in patient position using treatment monitoring software.

The limitations of this study include a small sample size, the treatment of normal animals, and inadequate immobilization of one animal. Using normal animals indirectly demonstrates the pain management capabilities of MRgFUS in MB nerve ablation. Inadequate immobilization resulted in the shift of the lesions away from the targets reducing the number of histologically evaluated cases from 24 to 19.

In conclusion, this preclinical study demonstrates the feasibility and safety of using MRgFUS for direct targeting of the lumbar MB nerve. The encouraging findings of this study warrant additional investigation of the optimal treatment parameters and should help advance the role of MRgFUS in treatment of low back pain. Furthermore, the results of this study may carry positive implications for expanding bone MRgFUS indications to include spine treatments.

Acknowledgments

We thank Donna M. Bouley, DVM, PhD (Professor, Department of Comparison Medicine, Stanford University) for valuable discussion of histological techniques, Lee-Ronn Paluch, DVM (Assistant Lab Member, Sloan Kettering Institute) for valuable discussion of pain assessment methods and James Keller (Memorial Sloan Kettering Cancer Center) for editorial assistance.

Dr. Stephen Solomon received research grant support from GE Healthcare. This work used core facilities funded by NIH Core Grant # P30 CA 008748.

References

1. Manchikanti L, Singh V, Pampati V, et al. Evaluation of the relative contributions of various structures in chronic low back pain. Pain Physician. 2001; 4(4):308–316. [PubMed: 16902676]
2. Cohen SP, Huang JH, Brummett C. Facet joint pain—advances in patient selection and treatment. Nature Reviews Rheumatology. 2013; 9(2):101–116. [PubMed: 23165358]

3. Tempany CM, Stewart EA, McDannold N, Quade BJ, Jolesz FA, Hynynen K. MR Imaging–guided Focused Ultrasound Surgery of Uterine Leiomyomas: A Feasibility Study 1. Radiology. 2003; 226(3):897–905. [PubMed: 12616023]
4. Hynynen K, Pomeroy O, Smith DN, et al. MR Imaging-guided Focused Ultrasound Surgery of Fibroadenomas in the Breast: A Feasibility Study. Radiology. 2001; 219(1):176–185. [PubMed: 11274554]
5. Ghai S, Louis AS, Van Vliet M, et al. Real-Time MRI-Guided Focused Ultrasound for Focal Therapy of Locally Confined Low-Risk Prostate Cancer: Feasibility and Preliminary Outcomes. American Journal of Roentgenology. 2015; 205(2):W177–W184. [PubMed: 26204305]
6. Martin E, Jeanmonod D, Morel A, Zadicario E, Werner B. High-intensity focused ultrasound for noninvasive functional neurosurgery. Ann Neurol. 2009; 66(6):858–861. [PubMed: 20033983]
7. Gianfelice D, Gupta C, Kucharczyk W, Bret P, Havill D, Clemons M. Palliative Treatment of Painful Bone Metastases with MR Imaging–guided Focused Ultrasound 1. Radiology. 2008; 249(1):355–363. [PubMed: 18695209]
8. Foley JL, Little JW, Vaezy S. Image-guided high-intensity focused ultrasound for conduction block of peripheral nerves. Ann Biomed Eng. 2007; 35(1):109–119. [PubMed: 17072498]
9. Lee Y-F, Lin C-C, Cheng J-S, Chen GS. High-intensity focused ultrasound attenuates neural responses of sciatic nerves isolated from normal or neuropathic rats. Ultrasound Med Biol. 2015; 41(1):132–142. [PubMed: 25438842]
10. Koopmann M, Shea J, Kholmovski E, et al. Renal sympathetic denervation using MR-guided high-intensity focused ultrasound in a porcine model. Journal of therapeutic ultrasound. 2016; 4(1):1–10. [PubMed: 26788322]
11. Kaye EA, Gutta NB, Monette S, et al. Feasibility Study on MR-Guided High-Intensity Focused Ultrasound Ablation of Sciatic Nerve in a Swine Model: Preliminary Results. Cardiovasc Intervent Radiol. 2015; 38(4):985–992. [PubMed: 26040256]
12. Huisman M, Staruch RM, Ladouceur-Wodzak M, et al. Non-Invasive Targeted Peripheral Nerve Ablation Using 3D MR Neurography and MRI-Guided High-Intensity Focused Ultrasound (MR-HIFU): Pilot Study in a Swine Model. PLoS One. 2015; 10(12):e0144742. [PubMed: 26659073]
13. Gulati A, Loh J, Gutta NB, et al. Novel use of noninvasive high-intensity focused ultrasonography for intercostal nerve neurolysis in a swine model. Reg Anesth Pain Med. 2014; 39(1):26–30. [PubMed: 24317231]
14. Harnof S, Zibly Z, Shay L, et al. Magnetic resonance-guided focused ultrasound treatment of facet joint pain: summary of preclinical phase. Journal of therapeutic ultrasound. 2014; 2(1):9. [PubMed: 24921048]
15. Weeks EM, Platt MW, Gedroyc W. MRI-guided focused ultrasound (MRgFUS) to treat facet joint osteoarthritis low back pain—case series of an innovative new technique. Eur Radiol. 2012; 22(12):2822–2835. [PubMed: 22935902]
16. White D, Clark J, Chesebrough J, White M, Campbell J. Effect of the skull in degrading the display of echoencephalographic B and C scans. The Journal of the Acoustical Society of America. 1968; 44(5):1339–1345. [PubMed: 5699038]
17. Fry F. Transkull transmission of an intense focused ultrasonic beam. Ultrasound Med Biol. 1977; 3(2):179–184. [PubMed: 595211]
18. Dupuy DE, Hong R, Oliver B, Goldberg SN. Radiofrequency ablation of spinal tumors: temperature distribution in the spinal canal. American Journal of Roentgenology. 2000; 175(5): 1263–1266. [PubMed: 11044019]
19. Vanderschueren GM, Obermann WR, Dijkstra SP, Taminiau AH, Bloem JL, van Erkel AR. Radiofrequency ablation of spinal osteoid osteoma: clinical outcome. Spine. 2009; 34(9):901–903. [PubMed: 19360000]
20. van der Linden E, Kroft LJ, Dijkstra PS. Treatment of vertebral tumor with posterior wall defect using image-guided radiofrequency ablation combined with vertebroplasty: preliminary results in 12 patients. J Vasc Interv Radiol. 2007; 18(6):741–747. [PubMed: 17538136]
21. Chhabra A, Andreisek G, Soldatos T, et al. MR neurography: past, present, and future. American Journal of Roentgenology. 2011; 197(3):583–591. [PubMed: 21862800]

22. Ishihara Y, Calderon A, Watanabe H, et al. A precise and fast temperature mapping using water proton chemical shift. Magn Reson Med. 1995; 34(6):814–823. [PubMed: 8598808]
23. Stasiak KL, Maul D, French E, Hellyer PW, Vandewoude S. Species-specific assessment of pain in laboratory animals. Journal of the American Association for Laboratory Animal Science. 2003; 42(4):13–20.
24. Bogduk N, Long DM. The anatomy of the so-called"articular nerves" and their relationship to facet denervation in the treatment of low-back pain. J Neurosurg. 1979; 51(2):172–177. [PubMed: 156249]
25. Scott SJ, Salgaonkar V, Prakash P, Burdette EC, Diederich CJ. Interstitial ultrasound ablation of vertebral and paraspinal tumours: Parametric and patient-specific simulations. Int J Hyperthermia. 2014; 30(4):228–244. [PubMed: 25017322]
26. Rodrigues DB, Stauffer PR, Vrba D, Hurwitz MD. Focused ultrasound for treatment of bone tumours. Int J Hyperthermia. 2015; 31(3):260–271. [PubMed: 25825987]
27. Bucknor MD, Rieke V, Seo Y, et al. Bone Remodeling after MR Imaging–guided High-Intensity Focused Ultrasound Ablation: Evaluation with MR Imaging, CT, Na18F-PET, and Histopathologic Examination in a Swine Model. Radiology. 2014; 274(2):387–394. [PubMed: 25302829]
28. Merlini L, Viallon M, De Coulon G, Lobrinus JA, Vargas MI. MRI neurography and diffusion tensor imaging of a sciatic perineuroma in a child. Pediatr Radiol. 2008; 38(9):1009–1012. [PubMed: 18581107]
29. Robbins N, Benedetti N, Scott B, Chin C, Douglas V. Magnetic Resonance Neurography in the Diagnosis of Noncompressive Lumbosacral Radiculoplexus Neuropathies (P5. 078). Neurology. 2015; 84(14 Supplement):P5. 078.

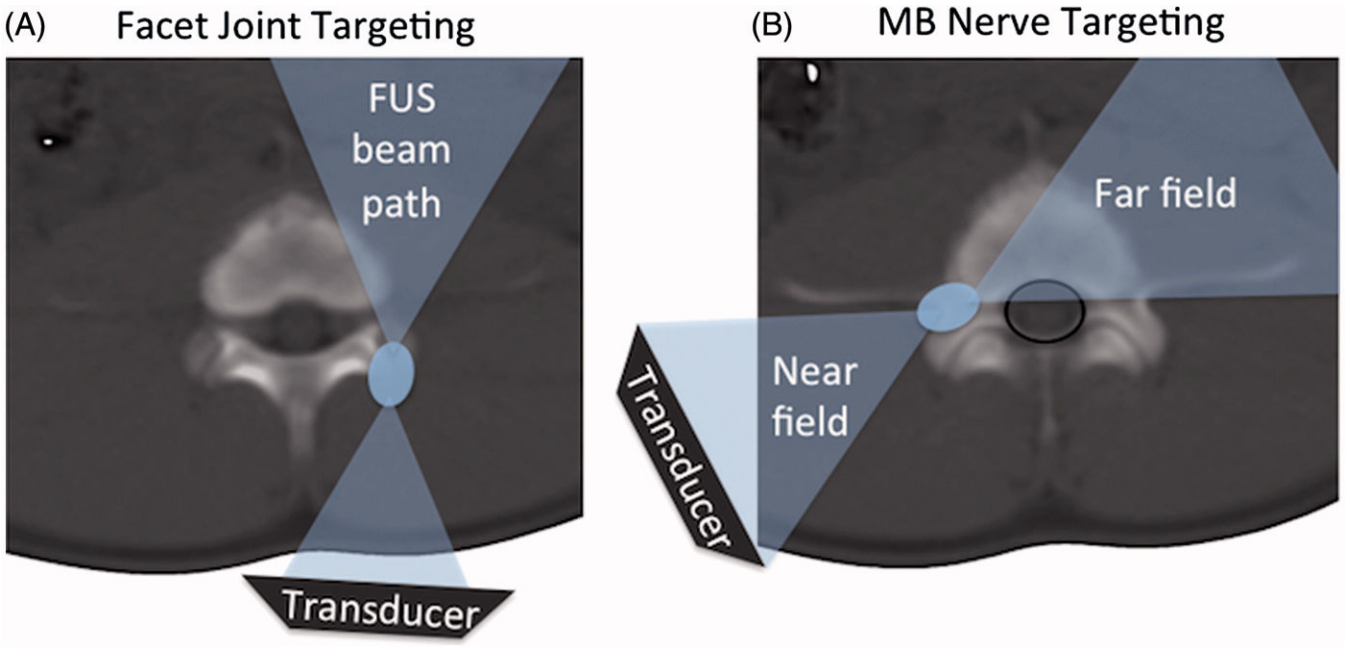

Figure 1.

A. Schematic of facet joint FUS ablation, showing the FUS beam (blue) aimed at the surface of the facet joint, and the far field of the beam aimed away from the spinal cord. B. Schematic of the proposed FUS ablation approach with direct targeting of the MB nerve and far field area and spinal canal (black line) partially overlapping.

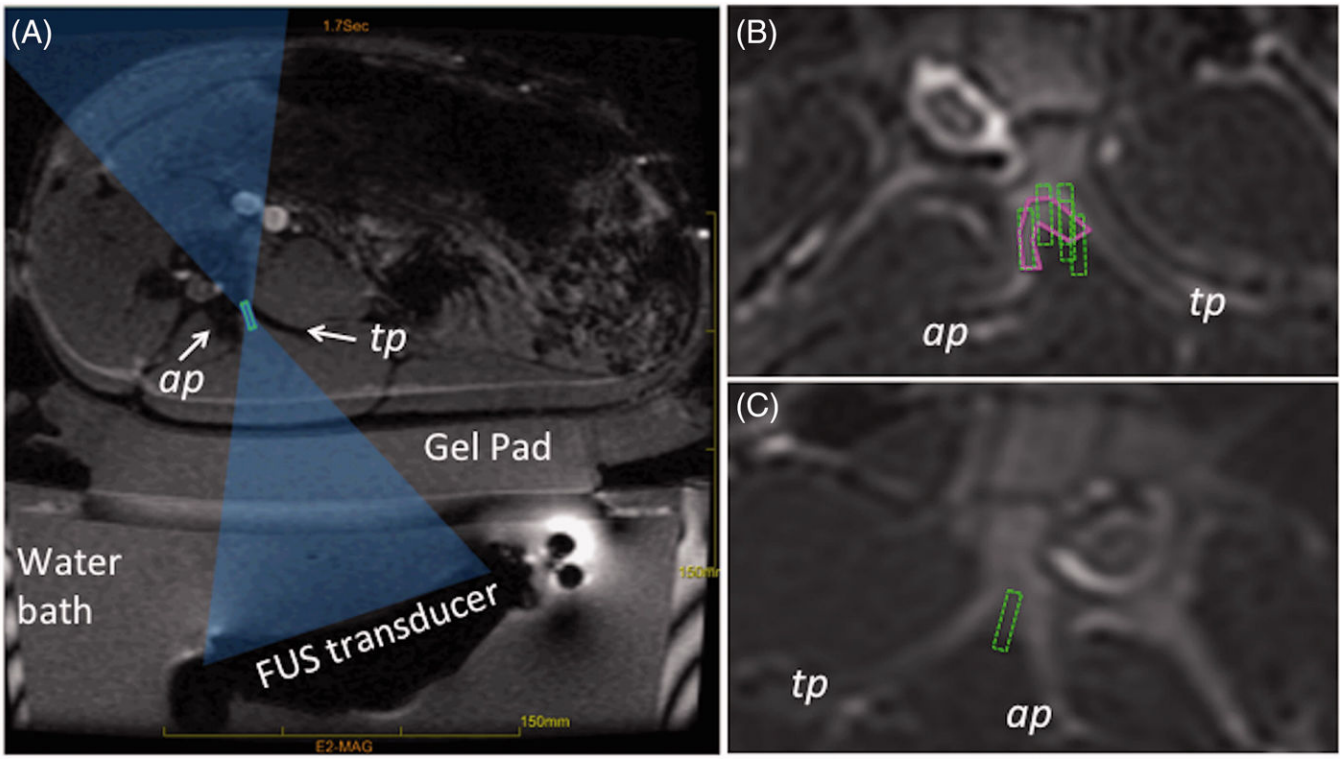

Figure 2.

A. Schematic of a FUS treatment setup showing the axial MR image of the setup with a swine positioned on top of the gel pad and the FUS beam focus (green rectangle) placed between the articular and transverse processes (labelled as *ap* and *tp*). The FUS beam is aimed directly at the MB nerve. B. Example of region-of-treatment contour (solid magenta contour) drawn by the operator during the planning phase. Dashed green rectangles represent the focal regions of the individual sonications automatically prescribed by the planning software. C. Example of planning where no region of treatment was prescribed and instead each sonication's focal region (dashed green rectangle) was individually placed by the operator.

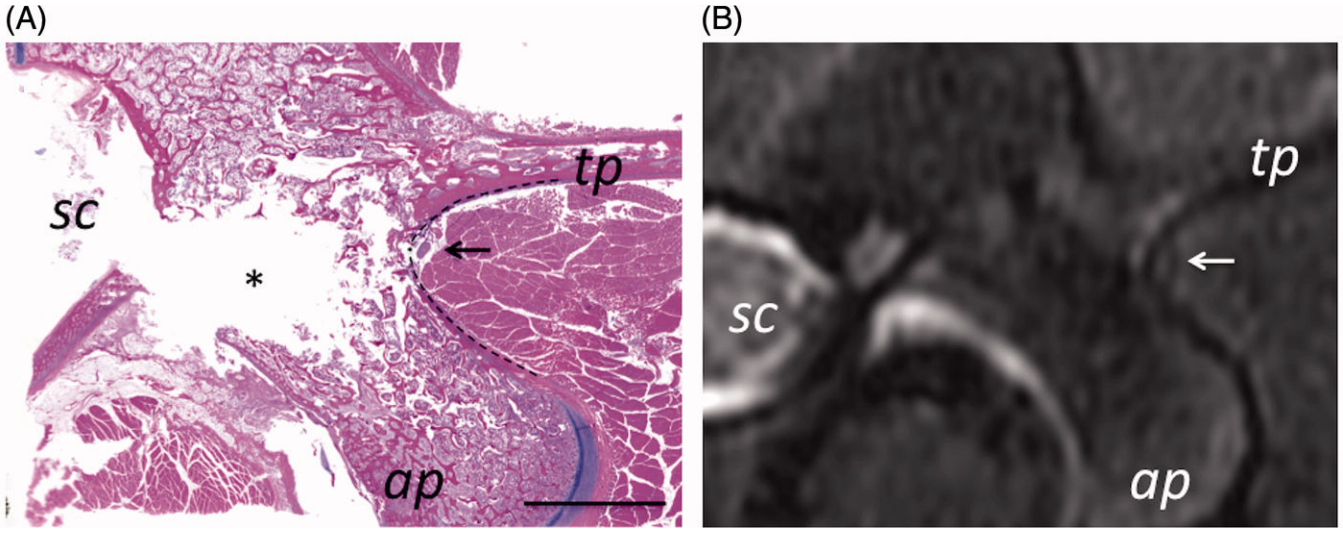

Figure 3.

MB nerve in Yorkshire swine was found to pass adjacent to the bone at the junction of the transverse and articular processes (labeled *tp* and *ap*). On histology (A), the nerve is seen surrounded by a layer adipose tissue (arrow). Scale bar is 1 cm. On MRI (B), a small hyper intense region surrounded by a hypo intense rim (arrow) corresponds to the position of the nerve determined from histology. Location of spinal cord is labeled as *sc*.

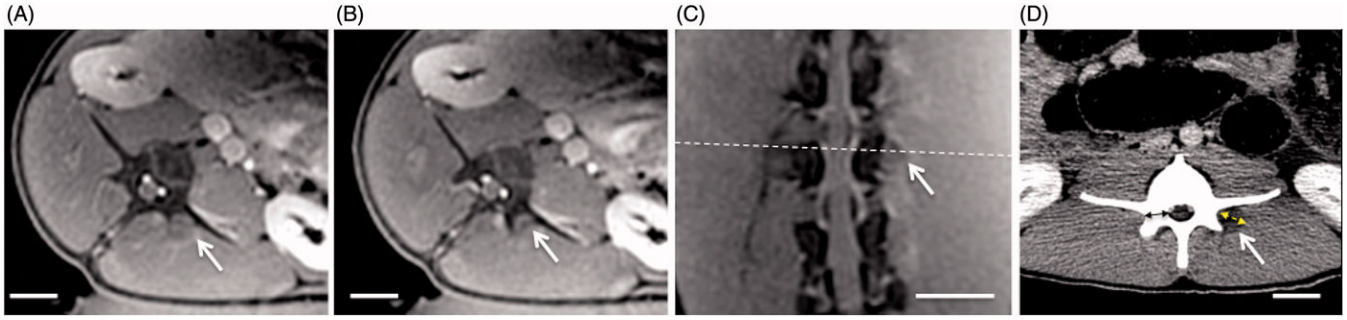

Figure 4.

Follow-up contrast-enhanced cropped MR and CT images from subacute experiment 1, showing the changes in contrast uptake from ablation of the vertebral level target at L4 using 9 sonications. Location of the axial slice (A) is shown with white dashed line on the oblique coronal image (C), and the axial slice shown in (B) is positioned adjacent and caudal to slice in A. Thermal lesions appear as non-enhancing areas (white arrows) due to the lack of perfusion resulting from thermal damage. The dashed double-sided arrow in D shows the measurement of the extent of the lesion along the hypotenuse between the transverse and articular processes as reported in Table 1. The solid double-sided arrow shows the measurement of the thickness of the pedicle bone. Scale bar is 2 cm.

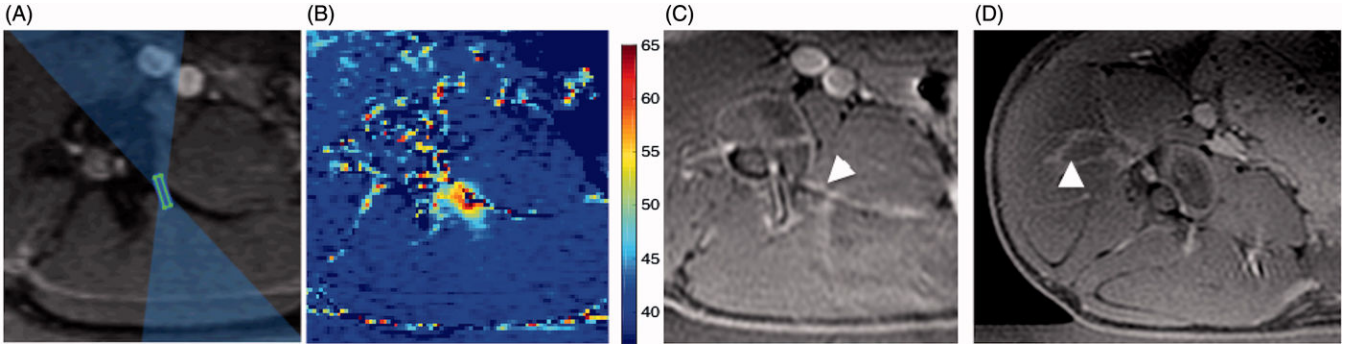

Figure 5.

A–C: Example of heating of transverse process in acute experiment 2. A. Cropped magnitude image of the MR thermometry sequence with an overlay of the focal spot and the beam path, as displayed by the planning software. B. Peak temperature that resulted from a sonication planned in A with acoustic energy 646 J (acoustic power of 32 W and sonication duration of 20 s). Highest temperature was 63 C. Contrast-enhanced MR image showing a hypo intense region at the edge of the transverse process (arrowhead) corresponding to the location of heating in B. D. Follow-up contrast-enhanced MR image from acute experiment 3, showing the lesion, non-enhancing region labeled with arrowhead, which shifted away from the MB nerve due to the shift of the animal position

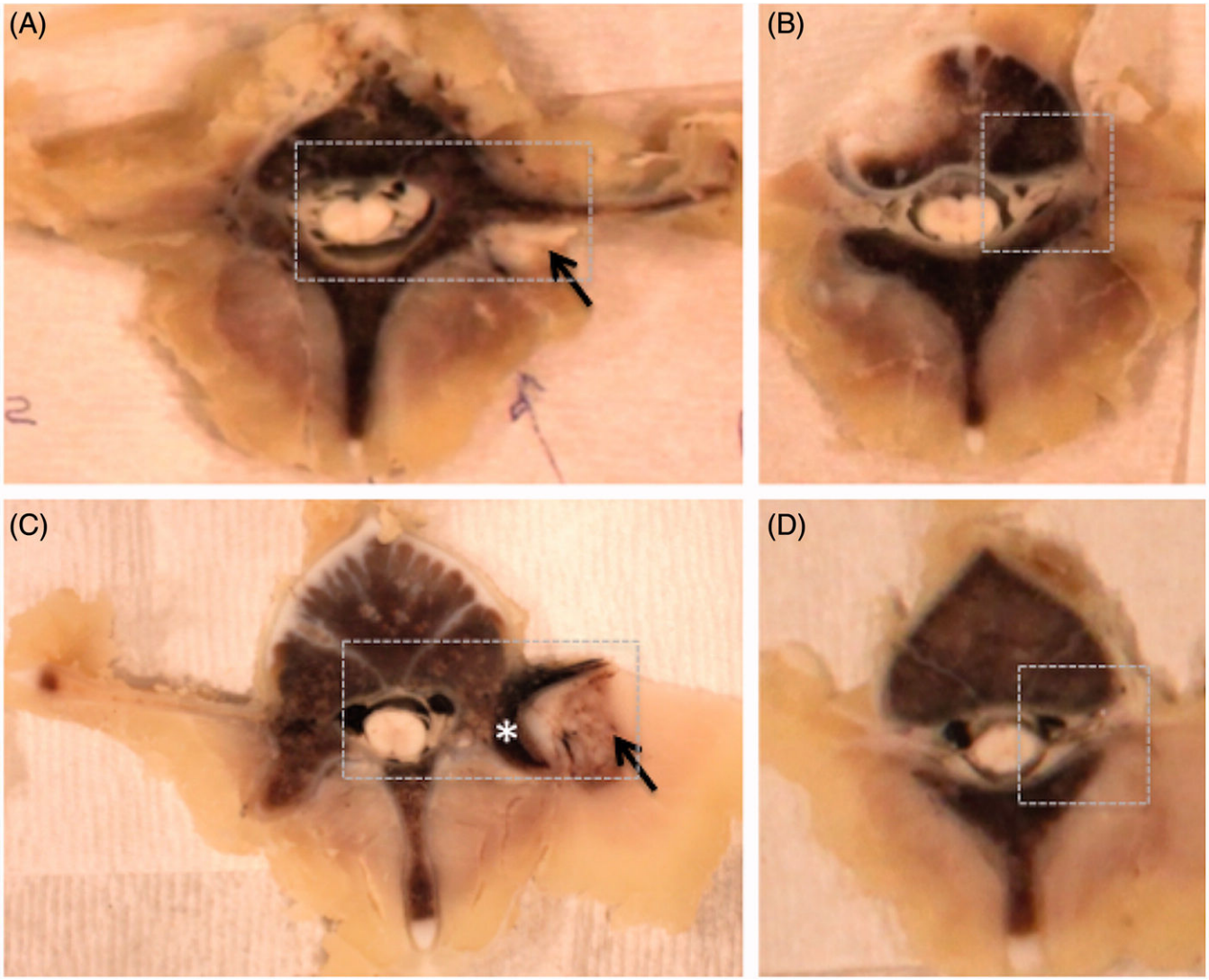

Figure 6.

Examples of gross pathology from the acute experiment 2 and subacute experiment 1. Ablation in muscle tissue (black arrow) appears as a paler area in the acute case (A-B) and the area surrounded by the brown rim in the subacute case (C–D). The brown rim of hemorrhage is apparent in the superficial region of the bone (asterisk) in the subacute case (C). The nerve roots, superior to the ablations, appear normal on gross pathology (B, D). The dashed box shows the region selected for histological analysis. Subacute gross pathology image corresponds to the follow-up images in Fig 4.

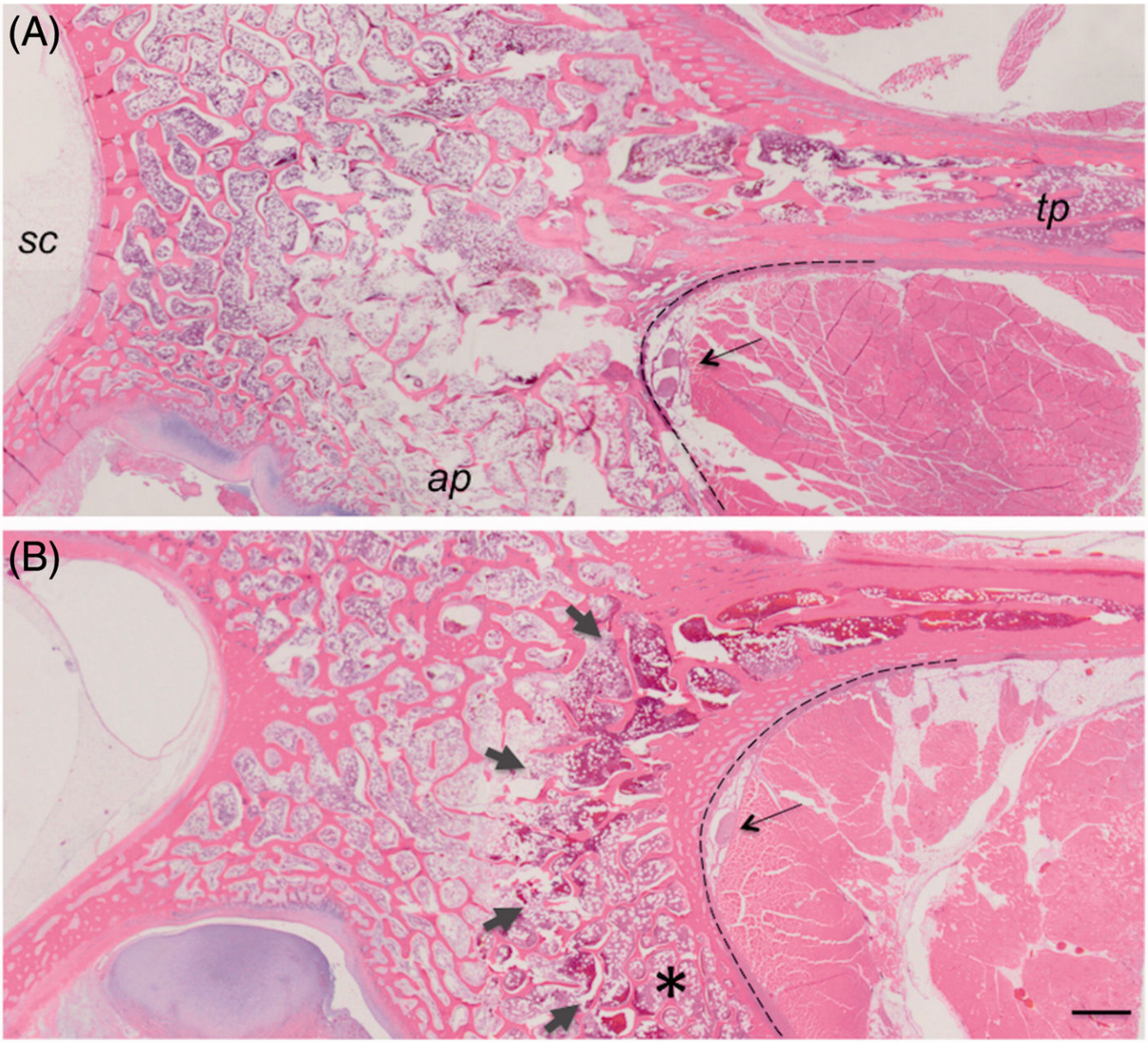

Figure 7.

Low magnification images of H&E histology from the acute (A) and subacute (B) studies. The dark red rim of hemorrhage (short arrows) visible at the surface of the bone between the articular process (*ap*) and transverse process (*tp*) made thermal lesions readily visible in subacute cases, compared to the acute cases. Changes in bone do not reach the spinal canal (*sc*). The nerve is shown with a long arrow. Dashed line delineates the interface between the bone and muscle. 1 mm scale bar.

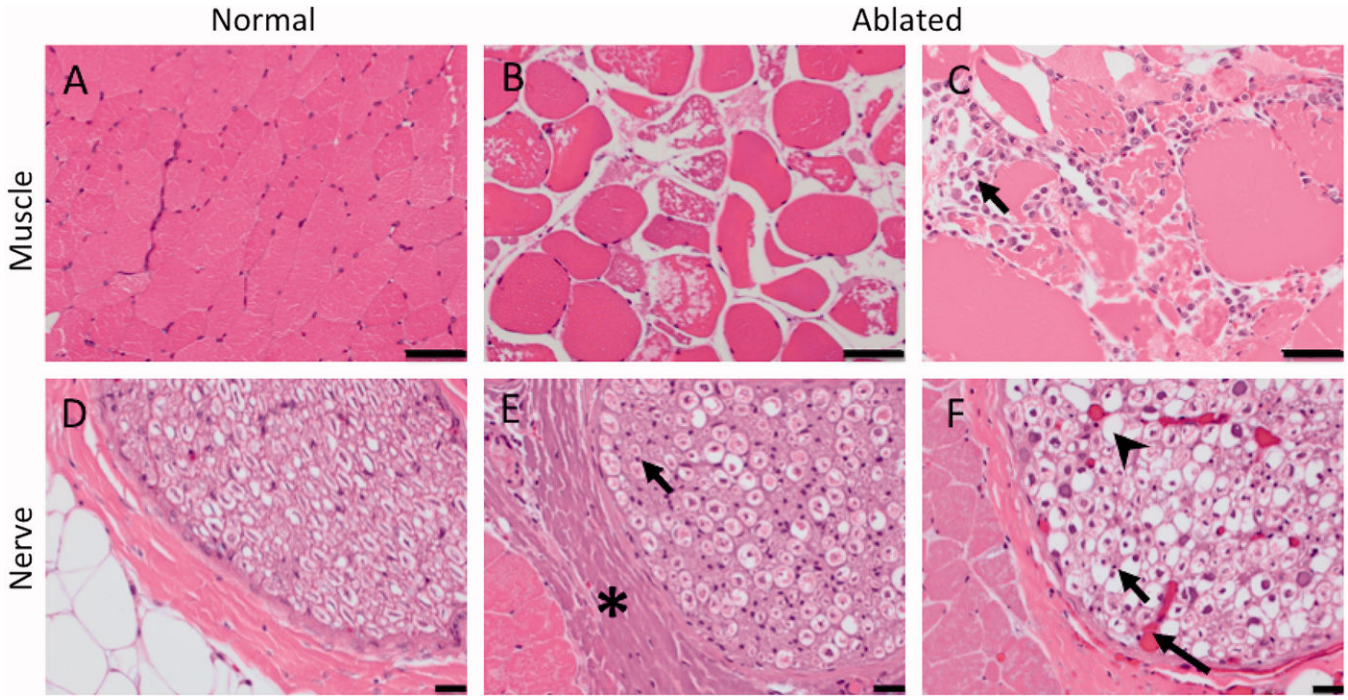

Figure 8.

H&E histology of the targeted nerve and adjacent muscle. Compared to normal muscle (A), ablated muscle showed swelling of muscle fibres, sarcoplasmic hypereosinophilia and fragmentation, and nuclear shrinkage (B) with macrophages present at the boundary of the lesion in subacute cases (arrow, C). 50 μm scale bar. Compared to the control nerve (D), the ablated nerve exhibited at least one, and often a combination, of the following changes: hyalinization of epineurial collagen (asterisk, E), nuclear shrinkage (arrow, E, F), hyperemia of endoneurial vessels (long arrow, F), and loss of axons associated with dilation of the myelin sheath (arrowhead, F). 20 μm scale bar.

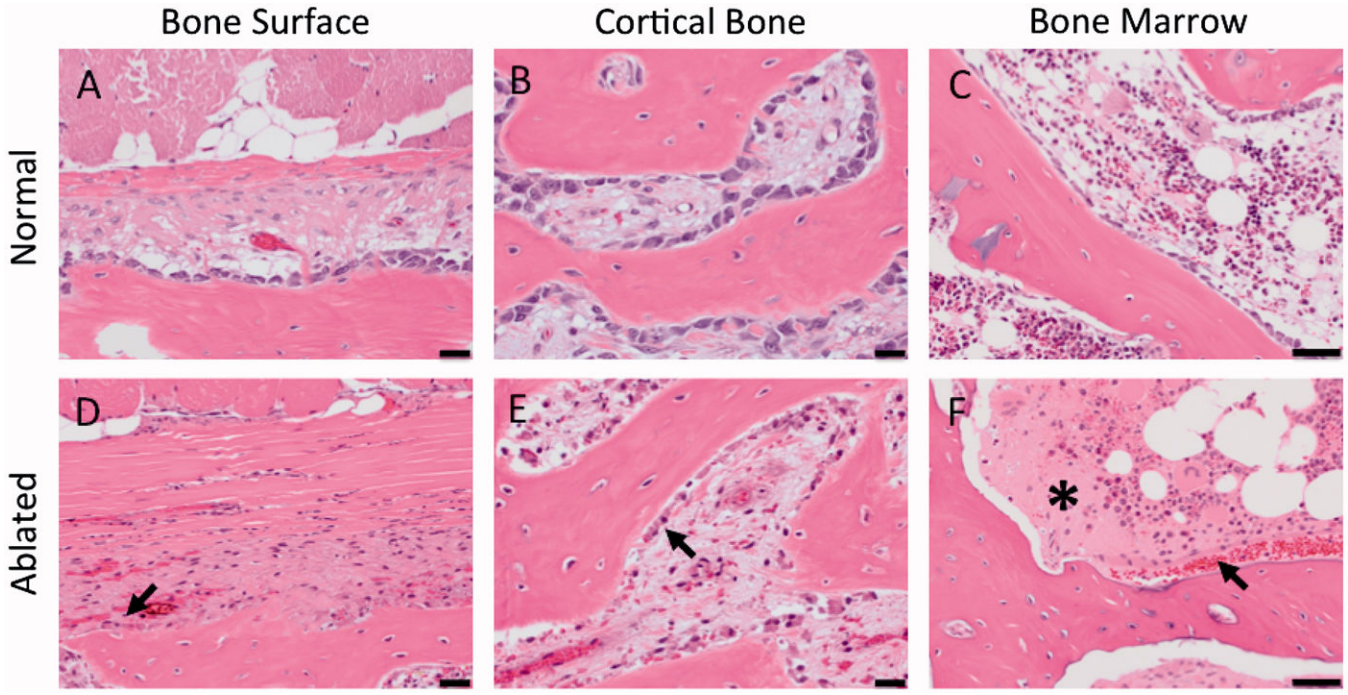

Figure 9.

H&E histology showing the cellular changes in the bone adjacent to the ablated MB nerve. Compared to control tissue, ablated bone had the following changes: shrinkage of osteoblasts (arrow, D, E) and increased eosinophilia of the extracellular spaces (asterisk) and hemorrhage (arrow) in bone marrow (F). 50 μm scale bar.

Table 1

Summary of the in vivo acute and subacute (S-Acute) experiments.

	Acute 1	Acute 2	Acute 3	S-Acute 1	S-Acute 2	S-Acute 3
Targeted levels	L4 – L6	L2 – L5	L3 – L5	L3 – L6	L3 – L4	L3 – L5
Sonications per targeted level (min-max)	4 – 6	4 – 8	1 – 6	7 – 9	5	3 – 4
Acoustic energy (J), median	693	646	913	627	707	708
Acoustic energy (J), (min-max)	422 – 727	619 – 742	822 – 1246	502 – 627	636 – 707	590 – 708
Average * acoustic energy (J), (min-max)	643 – 699	634 – 705	903 – 1246	550 – 619	693 – 707	634 – 708
Peak temperature ** (°C), median (min-max)	57.5 (49 – 72)	67 (49 – 87)	56 (42 – 72)	55 (42 – 79)	57 (52 – 64)	62 (51 – 73)
Average * peak temperature ** (°C), (min - max)	59 – 63	61 – 76	50 – 67	55 – 58	57 – 64	61 – 65
Lesion size (cm), (min - max)	0.6 – 1.6	0.8 – 1.6	1.9 – 2.6	0.9 – 1.4	1.1 – 1.3	0.9 – 1.3

*: Asterisk indicates values averaged across all sonications per targeted level.

**: Double asterisk indicates the temperature that was measured in muscle tissue adjacent to the bone.